Exchange Coupling Interactions from the Density Matrix Renormalization Group and *N*-Electron Valence Perturbation Theory: Application to a Biomimetic Mixed Valence Manganese Complex

Michael Roemelt,[a,b*] *Vera Krewald,*[c*] *Dimitrios A. Pantazis*[d*]

[a] Lehrstuhl für Theoretische Chemie, Ruhr-University Bochum, 44780 Bochum, Germany.

[b] Max Planck Institute for Coal Research, Kaiser-Wilhelm-Platz 1, 45470 Mülheim an der Ruhr, Germany.

[c] Department of Chemistry, University of Bath, Bath BA2 7AY, United Kingdom.

[d] Max Planck Institute for Chemical Energy Conversion, Stiftstraße 34-36, 45470 Mülheim an der Ruhr, Germany.

michael.roemelt@theochem.rub.de, v.krewald@bath.ac.uk, dimitrios.pantazis@cec.mpg.de

ABSTRACT

The accurate description of magnetic level energetics in oligonuclear exchange-coupled transition metal complexes remains a formidable challenge for quantum chemistry. The density matrix renormalization group (DMRG) brings such systems for the first time easily within reach of multireference wave function methods by enabling the use of unprecedentedly large active spaces. But does this guarantee systematic improvement in predictive ability, and if so, under which conditions? We identify operational parameters in the use of DMRG using as a test system an experimentally characterized mixed valence bis-μ-oxo/μ-acetato Mn(III,IV) dimer, a model for the oxygen-evolving complex of photosystem II. A complete active space of all metal 3d and bridge 2p orbitals proved to be the smallest meaningful starting point; this is readily accessible with DMRG and greatly improves on the unrealistic metal-only configuration interaction or complete active space self-consistent field (CASSCF) values. Orbital optimization is critical for stabilizing the antiferromagnetic state, while a state-averaged approach over all spin states involved is required to avoid artificial deviations from isotropic behavior that are associated with state-specific calculations. Selective inclusion of localized orbital subspaces enables probing the relative contributions of different ligands and distinct superexchange pathways. Overall, however, full-valence DMRG-CASSCF calculations fall short from providing a quantitative description of the exchange coupling owing to insufficient recovery of dynamic correlation. Quantitatively accurate results can be achieved through a DMRG implementation of second order *N*-electron valence perturbation theory (NEVPT2) in conjunction with a full-valence metal and ligand active space. Perspectives for future applications of DMRG-CASSCF/NEVPT2 to exchange coupling in oligonuclear clusters are discussed.

1. INTRODUCTION

Cluster complexes containing multiple magnetically coupled transition metal ions have received intense and sustained attention from experiment and theory alike.[1-5] For example, oligonuclear systems of magnetically interacting manganese ions feature prominently in fields as diverse as single-molecule magnetism[6-9] and photosynthetic water oxidation.[10-16] First-principles computational description of low-lying spin states in exchange-coupled transition metal systems has been so far dominated by density functional theory with the broken-symmetry approach (BS-DFT).[3, 17-30] The broken-symmetry solutions are not spin eigenstates and cannot be used directly for any comparisons with experiment, but the BS-DFT energies can be used to extract pairwise exchange coupling constants J_{ij} to be substituted into an appropriate phenomenological Heisenberg–Dirac–van Vleck Hamiltonian (Eq. 1).[30-32]

$$\hat{H}_{\mathrm{HDvV}} = -2\sum_{i<j} J_{ij}\hat{S}_i\hat{S}_j \qquad (1)$$

The exchange coupling constants J_{ij} parameterize the fictitious interactions between the different spin sites and hence determine the relative spin state energies of the coupled system. Appropriate spin projection techniques may enable the use of a specific BS-DFT solution for predicting various spin-dependent spectroscopic observables of the real system.[33]

Although its practical utility is undeniable, the standard BS-DFT approach has weaknesses and shortcomings that relate to the formally deficient treatment of an intrinsically multireference problem, the dependence on the nature of the chemical system, and the sensitivity to the choice of density functional.[27, 34-37] Other DFT-based approaches are being actively pursued.[29, 38-44] Wave function based methods have been successfully employed only for a comparatively limited number of simple systems with few unpaired electrons. The use of multireference methods that address the static correlation problem,[45] such as the complete active space self-consistent field (CASSCF), to directly obtain the energies of spin levels in magnetically coupled systems would be the most desirable foundation for

tackling such problems, but their application is severely restricted by their computational cost. Methods that account for dynamic correlation on top of a minimal active space have been explored. Among them, difference dedicated configuration interaction (DDCI) has been shown to offer an elegant and systematic way towards accurate results,[46-50] but the applicability of such methods is still strictly constrained by their explosive cost with increasing number of unpaired electrons and the fact that high-order excitations are indispensable in magnetic coupling problems.[51-52]

The obstacle to the use of sufficiently extended active spaces can potentially be lifted with the density matrix renormalization group (DMRG).[53-56] In the context of quantum chemistry, DMRG has emerged as a powerful algorithm that enables multireference calculations with significantly larger active spaces than ever before.[57-61] This is achieved by representing the wave function as a tensor network and constructing it from matrix products so that efficient mathematical formalisms can be exploited resulting in polynomial rather than exponential algorithmic scaling. The applicability of DMRG to transition metal chemistry has been explored in a number of recent studies.[62-68] A few reports have described DMRG-based calculations on transition metal clusters containing up to four open-shell (Mn or Fe) ions,[69-70] however without explicitly addressing the problem of exchange coupling. Pilot studies of binuclear and tetranuclear iron-sulfur model clusters[71] as well as of two simple quasi-linear Fe and Cr dimers with a single oxo bridge[72] showcased the feasibility of DMRG calculations for this problem, but the results highlighted uncertainties with respect to methodological requirements and the role of dynamic correlation. The performance of the approach and the necessary conditions for its successful application remain poorly defined.

In the present work we investigate how DMRG can be used to obtain exchange coupling constants in combination with complete active space configuration interaction (CASCI) and CASSCF approaches on large active spaces. We use an experimentally characterized manganese complex of known structure and

magnetic properties, an antiferromagnetically coupled mixed-valence bis-μ-oxo/μ-acetato Mn(III,IV) dimer.[73] Magnetic properties of cluster complexes with magnetically interacting Mn ions bridged by multiple oxo and carboxylato bridges have long been studied,[5, 14, 74-83] owing to their direct relevance to single molecule magnets and the water-oxidizing Mn_4CaO_5 cluster of biological photosynthesis, so the present complex can be considered an archetypal model for a wide variety of larger systems. We establish the dependence of exchange coupling on active space composition, orbital optimization, and number of renormalized states, determining the requirements for successful application of the method. DMRG allows us not only to simply include the orbitals of all bridging ligands in the active space, but also to selectively turn specific (super)exchange pathways on and off by choosing specific ligand-localized orbital subspaces. We demonstrate that this approach can be used to assess the role of each bridge in determining the sign and magnitude of the exchange coupling. Additionally, we evaluate the application of *N*-electron valence perturbation theory (NEVPT2)[84-85] coupled to large active space DMRG as a way to converge towards reliable recovery of dynamic correlation in the description of exchange coupling.

2. MODELS AND METHODS

2.1. Reference Model. Complex **1** (Figure 1) was reported by Wieghardt and coworkers.[73] It is a mixed valence bis-μ-oxo/μ-acetato Mn(III,IV) dimer with 1,4,7-trimethyl-1,4,7-triazacyclononane and acetates as terminal ligands. The metal oxidation states, bridging patterns, ligand types, and coordination geometries are relevant to manganese-based single-molecule magnets, but they also mimic those that occur in the OEC of photosystem II.[9-10, 86] Specifically, the Mn_4CaO_5 cluster of the enzyme is known to cycle from $Mn(III)_3Mn(IV)$ in the lowest oxidized state (S_0) up to an all-Mn(IV) form in the S_3 state that precedes the final, as yet unobserved, O_2-evolving transient state (S_4).[87-92] Mirroring the situation in the OEC, the Mn(III) ion of complex **1** features a strong axial pseudo-Jahn–Teller elongation that leads to an approximately square-pyramidal coordination geometry, precisely like the Mn(III) ions in the S_1 and S_2 states of the OEC.[93-95] The Mn ions in the OEC are similarly bridged by oxo and carboxylato bridges, while the ancillary ligands on the Mn(III) center of **1** also mimic the first coordination sphere of the OEC, which is rich in Glu and Asp residues.[95-97]

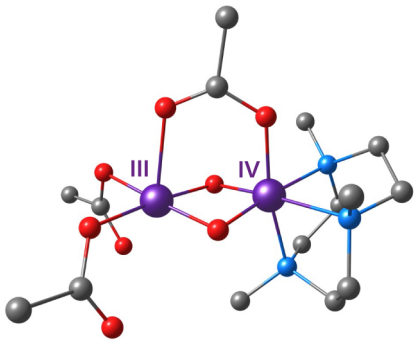

Figure 1. Structure of complex **1**. Mn purple, O red, N blue, C grey. Hydrogen atoms are omitted for clarity.

This is a rare example of a Mn dimer with crystallographically well-defined valence localization and Jahn–Teller distortion thanks to the asymmetric ligand environment of the two metal ions. Therefore, the crystallographic model (CSD access code KUVPEW) was employed directly after optimizing the hydrogen positions. Since **1** is neutral, there is no need to account for counterion effects. Additionally,

avoiding a charged system in the present case helps eliminate theoretical and computational complications that may manifest as convergence failures or negative ionization energies for anions. Magnetic susceptibility measurements showed that complex **1** is antiferromagnetically coupled and shows Heisenberg behavior with an exchange coupling constant $J = -90.0$ cm^{-1} (according to the Hamiltonian convention shown in Eq. 1).

2.2. Computational Details. All DFT and the majority of multireference (CASCI, CASSCF, and NEVPT2) calculations were performed with the ORCA program package[98] interfaced with the BLOCK code[55, 99-102] of Chan and coworkers for DMRG. In the case of DMRG-NEVPT2 calculations with an active space of 19 electrons in 16 orbitals we used the MOLBLOCK code developed by one of us (M. R.) that is also interfaced with the BLOCK code. DFT calculations used the TPSS functional[103] with D3BJ corrections[104-105] for geometry optimizations and the TPSSh,[106] BP86[107-108] and M06-2X[109] density functionals for calculation of exchange coupling constants, with tight convergence criteria and extra fine integration grids (Grid6 and GridX8), setting the overall radial integration accuracy to 6.0 in ORCA nomenclature. The zeroth order scalar relativistic approximation (ZORA)[110-114] was used in all calculations, in combination with the ZORA-adapted[115] and partially decontracted polarized triple-zeta def2-TZVP and doubly polarized quadruple-zeta def2-QZVPP basis sets,[116] and appropriate versions of corresponding auxiliary basis sets by Weigend[117] and Hättig.[118] Starting orbitals for DMRG calculations were obtained from Pipek–Mezey localization[119] of canonical or quasi-restricted[120] DFT orbitals. Automatic ordering of orbitals was performed with the Fiedler vector algorithm.[121-124] In the following we use the common nomenclature (N_{el}, N_{orb}) to denote the number of active space electrons and orbitals.

Since the optimal selection of the various methodological parameters that enter a DMRG calculation is one of the targeted outcomes of the present work, most of these details will be presented and discussed as needed in the following. The distinct difference in applications of DMRG to magnetic

coupling compared with many other situations in chemistry is that the target energy differences need to be determined with a precision on the order of a few wavenumbers (cm^{-1}). Most relevant for the convergence of the energy of any DMRG calculation is the number of states M retained during the renormalization step and the associated discarded weight. The latter corresponds to the difference between the trace of the active space density obtained from the renormalized wave function and an ideal value of 1. A commonly chosen approach to approximate the true full-CI energies from DMRG calculations is to perform a number of calculations with a varying number of retained states and then extrapolate to zero discarded weight. However, in the current investigation of magnetic couplings such a procedure is not viable since the obtained discarded weights (and their differences) are negligible (on the order of 10^{-15}) for all reported calculations and no systematic correlation between the energy convergence in the wavenumber regime and the largest discarded weight could be observed. Therefore the number of retained states was increased until convergence of the magnetic coupling constants on the order of 1 cm^{-1} was achieved.

For some active spaces the calculated DMRG energies were refined by taking into account dynamic electron correlation within the framework of second order *N*-electron valence perturbation theory (NEVPT2).[84-85] This widely used approach describes the influence of the first order interacting space[125] on the DMRG-CASSCF or DMRG-CASCI energy (and wave function) by means of second order perturbation theory. More precisely, we have used the strongly contracted variant of NEVPT2 as implemented for DMRG by Chan and coworkers.[126] As suggested previously the required active space reduced density matrices were generated using a compressed number of renormalized states.[126] This was achieved by carrying out a "reverse scheduled" set of sweeps, where the number of renormalized states is first increased to a maximum value of M = 2000 before it is reduced to a final value of M'.[127] A key ingredient of strongly contracted NEVPT2 is the orbital energies that enter the expressions for the

perturbed energy and wave function. In calculating multiple states with the largest active spaces reported in this work state-averaged orbitals were employed in NEVPT2 unless stated otherwise. Avoiding recanonicalization of the state-averaged CASSCF orbitals leads to practically identical results as the use of state-adapted orbitals in the present NEVPT2 calculations, because the states of different multiplicity arise from the same configuration. Note that although in the majority of the presented DMRG-CASSCF calculations the molecular orbitals are optimized in a state-averaged fashion, separate DMRG calculations were performed for each spin state.

3. RESULTS AND DISCUSSION

3.1. Exchange Coupling Constants from DFT. To have a measure of comparison of the DMRG values discussed in the following, we first describe some fundamental concepts and show what can be obtained with straightforward broken-symmetry DFT calculations. The two metal centers in complex **1** have local spins $S_A = 3/2$ and $S_B = 2$, for the d^3 and d^4 ions Mn(IV) and Mn(III). Coupling of the two spins yields total spin states $S = S_A + S_B, S_A + S_B - 1, \ldots, |S_A - S_B|$ and hence the Heisenberg spin ladder for the dimer is composed of the spin states S = 1/2, 3/2, 5/2, and 7/2.[128-129] If Eq. 1 applies then the energies follow a regular spacing provided by Eq. 2:

$$E(S) = -J[(S(S+1) - S_A(S_A+1) - S_B(S_B+1)] \quad (2)$$

and the sign of J determines whether S = 1/2 or S = 7/2 is the ground state. Thus, in the ideal isotropic case, the energy spacings between the four spin states for the present dimer are equal to 3J, 5J and 7J, from lowest to highest spin.[128-129] Multireference methods enable direct access to all these possible spin states. If these indeed conform to the Landé pattern of Eq. 2, then J can be determined by any energy difference between pairs of spin states. Alternatively, by solving Eq. 2 for J, a fitted exchange coupling constant can be obtained from the slope of a linear regression between $E(S)$ and $S(S+1)$. Departures from

isotropic behavior, for example due to double exchange, can also be determined by analyzing the complete energy spectrum obtained directly from multireference calculations.[71, 130]

On the other hand, the DFT-based approach to exchange coupling relies on calculation of the high-spin S = 7/2 state (note that no other spin state of the ladder can be approximated by a single determinant) and of a broken-symmetry solution with M_S = 1/2, obtained by "flipping" the spin of one ion while maintaining the local high-spin configurations.[3, 17-19, 25, 27, 32, 131-133] No other solution relevant to the magnetic coupling problem is possible. Convergence to the desired broken symmetry determinant is confirmed by the spin populations, close to 4 spin-up electrons for the Mn(III) site and 3 spin-down electrons for Mn(IV). This BS solution is not a spin eigenfunction and should not be confused with the S = 1/2 spin state mentioned above. Instead its computed energy can be used with an appropriate projection formula such as the Yamaguchi projection that weighs the energies of the high-spin and BS solutions by the spin expectation values to extract a J constant (Eq. 3),[134] which is subsequently used to reproduce the spin state ladder as described above. More complex treatments involving multiple BS solutions are used for higher nuclearity systems.[26, 33, 70, 83, 135-139]

$$J = -\frac{E_{\mathrm{HS}} - E_{\mathrm{BS}}}{\left\langle S^2 \right\rangle_{\mathrm{HS}} - \left\langle S^2 \right\rangle_{\mathrm{BS}}} \qquad (3)$$

In the present case this approach yields J = −161.7 cm^{-1} using the BP86 functional, J = −18.2 cm^{-1} with M06-2X, and J = −95.1 cm^{-1} with TPSSh, to be contrasted with the experimental value of −90.0 cm^{-1}.[73] These values highlight the strong dependence of exchange couplings on the choice of functional. In high-valent Mn systems it has been noted that the performance of the hybrid meta-GGA functional TPSSh is consistently reliable,[14, 33, 76-77, 89] at least partly owing to the moderate amount of exact exchange (10%). However, this is not a universally applicable recipe for any exchange coupled system. The fundamental weakness remains that BS-DFT cannot be systematically improved and conclusions regarding the optimal functional and its error margins are not transferable.

3.2. Multireference Treatment with Metal-only Active Space. The smallest chemically reasonable active space that can be used for a multireference description of complex **1** is a space composed of all unpaired electrons of the Mn ions distributed over the Mn 3d orbitals, i.e. a (7,10) active space (see Figure 2). Calculations with this active space were performed with traditional CASSCF and with DMRG-CASSCF and the results are identical already with a number of renormalized states $M = 500$. As a first step in the use of multireference methods we investigated a straightforward configuration interaction approach using Pipek–Mezey localized quasi-restricted orbitals from a DFT calculation. The (7,10) CI calculation resulted in a very large ferromagnetic coupling of $J = +179$ cm^{-1} (the same value is obtained regardless of the specific energy difference between states used) in profound disagreement with experiment. Staying within the confines of this minimal active space, we examined whether the reason for this failure could be the origin of localized orbitals by comparing results obtained using different source orbitals and localized orbitals derived from the alternative Foster–Boys localization scheme.[140] As these different choices did not introduce any delocalization, they also did not affect the exchange coupling qualitatively and therefore we conclude that a (7,10) CI description of the system with metal-based orbitals is fundamentally deficient.

Orbital optimization changes the picture drastically. The energies of individually optimized spin states do not follow a regular Landé pattern: the ground state is correctly predicted to be the low-spin, $S = 1/2$ state, but this is followed by the $S = 7/2$ at 12.1 cm^{-1}, $S = 3/2$ at 16.2 cm^{-1} and $S = 5/2$ at 27.9 cm^{-1}. This suggests that these state-specific CASSCF(7,10) calculations are not appropriate for discussing exchange coupling. We note that using a *single* set of orbitals optimized for either the high-spin ($S = 7/2$) or the low-spin ($S = 1/2$) state and determining the relative energies of the remaining states from CI calculations does not lead to meaningful results, because the corresponding state for which the orbitals are optimized always lies two to three thousand wavenumbers below the others.

In contrast, state-averaged (7,10) CASSCF results lead to a normal Landé distribution of spin states with an antiferromagnetic exchange coupling constant of −1.6 cm^{-1} with a spread of 0.2 cm^{-1} ($J_{(7/2–5/2)}$ = −1.5 cm^{-1}, $J_{(5/2–3/2)}$ = −1.6 cm^{-1}, and $J_{(3/2–1/2)}$ = −1.7 cm^{-1}). Note that under the assumption of Landé spacing one can use any pair of spin state energies to derive an effective *J* value, or a linear regression as mentioned above. For the four spin states in the present case there are six possible energy differences (three linearly independent ones) that can be used. The relative energies of all states are provided explicitly in the present work. To facilitate the discussion, *J* values obtained from energy differences between successive pairs of spin states (that is, doublet–quartet, quartet–sextet, and sextet–octet) are mentioned and the average of these three values is used as an effective *J* for a given method, while "spread" refers to the difference between the largest and smallest of these three successive *J* values and is a measure of deviations from the Landé pattern. Values of *J* obtained from linear fits as described in the previous section are also reported in the Supporting Information, along with associated R^2 values; they are consistent with the averaged *J* values reported in the main text.

The result of the CASSCF(7,10) calculation described above is that it introduces small delocalization "tails" to the starting tightly localized orbitals, that is, the final state-averaged CASSCF orbitals have non-zero amplitudes on the bridging ligands. Still, the numerical result is of no practical value. The importance of orbital choice in multireference calculations with a minimal active space has been discussed with respect to the delocalization on the bridging ligands and in relation to the relative description of neutral and ionic components of the wave function.[141-144] In a view that attempts to distinguish between metal-based magnetic orbitals as the basis for static correlation and everything else added on top as contributor to dynamic correlation, a minimal metal-based active space is seen as the starting point for subsequent dynamic correlation treatments like DDCI, which enables clearly distinguishable classes of excitations.[47, 49-52, 145] As an operational concept this is not applicable in the

present study, where we target active space expansion by virtue of the DMRG. Therefore in the following we extend the active space in a chemically motivated and systematic way that aims to directly incorporate the ligand contributions (ligand-to-metal charge transfer)[49, 145-147] to the magnetic coupling.

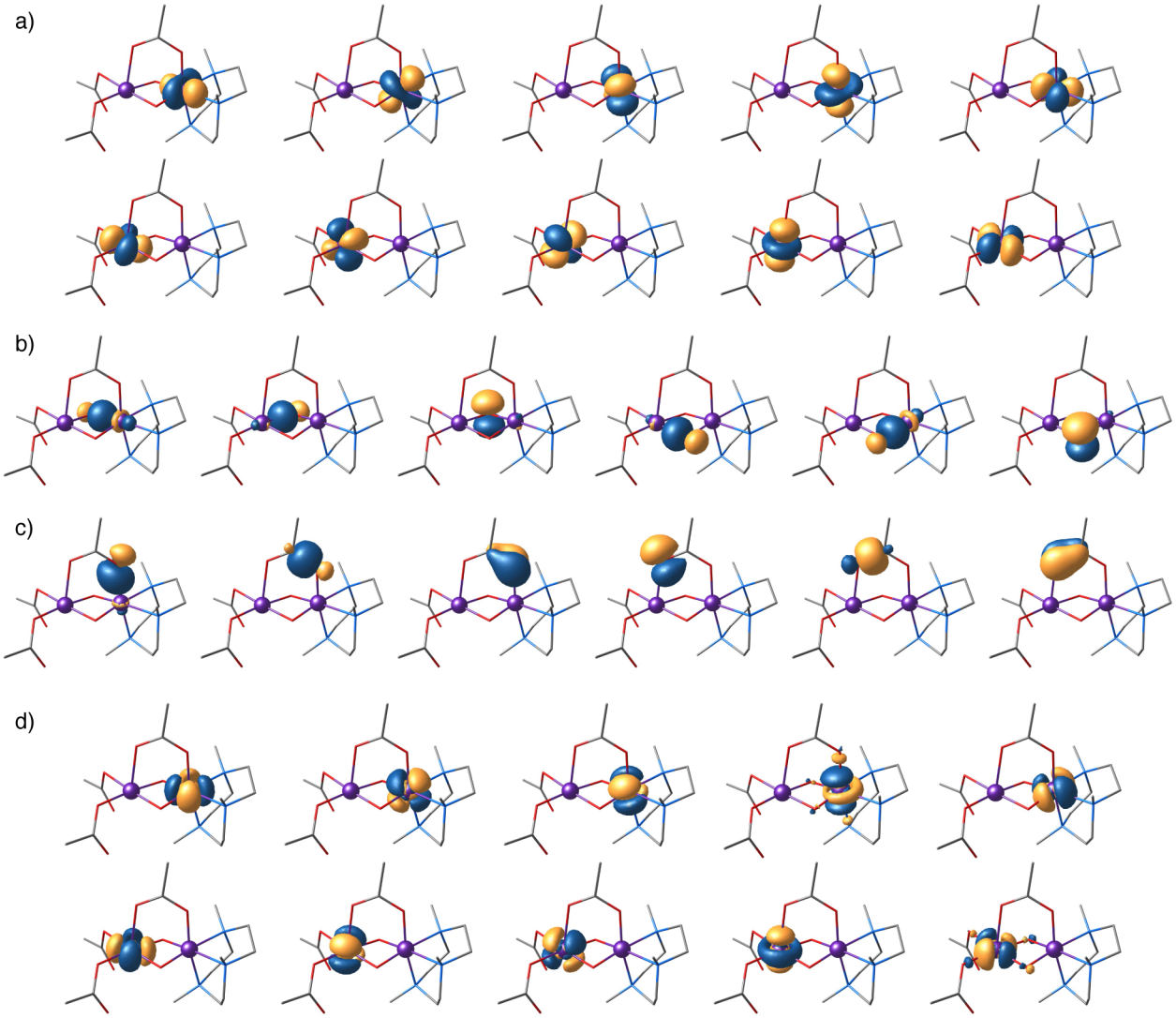

Figure 2. Main localized orbitals used for initial construction or extension of the active spaces described in the present work. a) Mn 3d orbitals, b) O 2p orbitals, c) OAc 2p orbitals, and d) Mn 4d orbitals.

3.3. Inclusion of Oxo Bridge Orbitals. Inclusion of the occupied 2p orbitals of the two oxo bridges (three orbitals for each O bridge) is expected to switch the superexchange mechanism on and thus enhance the antiferromagnetic coupling. This leads to a (19,16) active space. In the preceding section we showed that the direct use of metal 3d localized orbitals in a CI treatment resulted in a qualitatively

incorrect description of the system and an inverted spin ladder. It is useful to know whether orbital optimization might have a less profound effect if a more complete active space is used, so we first performed DMRG-CASCI calculations using the (19,16) active space consisting of localized Mn 3d orbitals and 2p oxo bridge orbitals. In this case all active space orbitals were derived simultaneously from the initial localization procedure. These DMRG-CASCI calculations still incorrectly predicted an inverted spin ladder with the high-spin $S = 7/2$ state as the ground state and yielded distinct deviations from Heisenberg behavior. The sextet, quartet and doublet states are located at 433 cm^{-1}, 897 cm^{-1} and 1324 cm^{-1} above the ground octet state (values identical to canonical CASCI at $M = 1500$). It is clear that the direct use of localized QROs in constructing the large active space and the lack of orbital optimization restrict the utility of this DMRG-CASCI approach for studying exchange coupling.

As a second step, we investigated the addition of localized O 2p orbitals on top of the previously optimized (7,10) Mn 3d orbitals, but without orbital reoptimization in the (19,16) active space. A DMRG-CASCI calculation with this type of active space yields a J of -28.8 cm^{-1}, drastically improving the (7,10) CASSCF result of $J = -1.6$ cm^{-1}. This value is converged at $M = 1000$. Finally, proceeding with orbital optimization using spin-state-averaged DMRG-CASSCF(19,16) calculations more than doubles the strength of antiferromagnetic coupling, leading to a J value of -59.0 cm^{-1}. The natural orbital occupation numbers for the O 2p orbitals deviate non-negligibly from 2.0 and are reduced to ca. 1.85 electrons for the in-plane orbitals that interact in a σ-fashion with the Mn(IV) center and 1.95 electrons for the other two. Although the predicted coupling still underestimates the experimental value, the result appears to finally provide a physically sound description of the system as it enables the inclusion of ligand-to-metal charge transfer that contributes to superexchange.[31, 52] Given that a convincing description of the system is obtained at this level, it is worth discussing a few methodological points in greater detail.

First of all, we note that DMRG-CASSCF requires a higher number of retained states than CASCI to achieve similar convergence, and this requirement increases with larger spaces. As a technical note, it proved most efficient to achieve convergence of DMRG-CASSCF by adding localized orbitals on top of pre-optimized orbital subspaces and directly starting with relatively high values for M, i.e. at least 1000. This avoids convergence problems observed in direct large-active-space use of localized orbitals, but also requires manual, chemically-driven construction of intermediate subspaces. Given the necessity for this type of manipulation and for orbital optimization, coupled to the fact that high starting M values may be required, it is not clear whether an automated orbital selection approach[148] that relies on analysis of preliminary orbitals at low M values would be of the same effectiveness here as in other applications.

Table 1 shows how the energy levels evolve with the number of renormalized states ranging from 250 to 3000. Smaller values of M either lead to scattered results or do not converge at all. The results obtained with M = 250 are unusable because there is no reasonable relationship between adjacent energy levels. In our opinion the results with M = 500 are also unusable, despite the fact that the average of the energy differences between adjacent levels does lead to the same value of J as the results with higher M values. From M = 1000 onwards the average J value is converged. The only differences are small improvements in the relative energy of the first excited state (S = 3/2), which result in restricting the differences between the three possible J values from 3.4 cm^{-1} (M = 1000) to 2.4 cm^{-1} (M = 3000).

Inclusion of the O 2s orbitals was also evaluated as an extension of the above results. The corresponding DMRG-CASCI calculations with an (23,18) active space showed no further effect on the exchange coupling (J = −58.5 cm^{-1}). The (19,16) active site was deemed appropriate to test possible basis sets effects, so DMRG-CASSCF calculations were repeated (starting from the initial localization setup up to the construction of the final active space) using the more extensively polarized ZORA-recontracted def2-QZVPP basis sets for Mn and O. Similarly to the known weak basis set dependence of

classical CASSCF, the DMRG-CASSCF results also proved insensitive. Compared to the results reported in Table 1, the def2-QZVPP values deviated by ca. 1 cm^{-1} for equivalent M values.

Table 1. Energy level differences in cm^{-1} between spin states computed from state-averaged DMRG-CASSCF calculations on complex **1** with a (19,16) active space composed of Mn 3d and O 2p orbitals for different numbers of renormalized states M, corresponding exchange coupling constants derived from energy differences of adjacent spin levels, and average J value (cm^{-1}).

S	M = 250	M = 500	M = 750	M = 1000	M = 1500	M = 2000	M = 2500	M = 3000
7/2	775.3	868.2	876.7	878.7	879.6	879.9	879.9	879.9
5/2	694.8	486.3	477.6	476.3	475.9	475.9	475.9	475.9
3/2	490.1	215.0	186.0	182.6	181.0	180.6	180.5	180.4
1/2	0.0	0.0	0.0	0.0	0.0	0.0	0.0	0.0
$J_{(7/2–5/2)}$	-11.5	-54.6	-57.0	-57.5	-57.7	-57.7	-57.7	-57.7
$J_{(5/2–3/2)}$	-40.9	-54.3	-58.3	-58.7	-59.0	-59.1	-59.1	-59.1
$J_{(3/2–1/2)}$	-163.4	-71.7	-62.0	-60.9	-60.3	-60.2	-60.2	-60.1
J	-71.9	-60.2	-59.1	-59.0	-59.0	-59.0	-59.0	-59.0

The convergence of absolute energies (Table S1) shows that individual states are stabilized with increasing M as expected, but to different extents. Comparison of the M = 1000 total energies with those obtained with M = 250 show that the S = 7/2 state is lowered by 26.2 cm^{-1}, whereas the S = 5/2, 3/2 and 1/2 states are respectively stabilized by 348.0 cm^{-1}, 437.0 cm^{-1} and 129.5 cm^{-1}. Comparison of M = 1000 and M = 2000 results shows much smaller change in total energies by 0.4 cm^{-1}, 2.0 cm^{-1}, 3.7 cm^{-1}, and 1.6 cm^{-1}. Finally, at M = 3000 there is a further minute stabilization of the S = 3/2 state by 0.2 cm^{-1}, whereas the energies of all other states are affected by less than 0.1 cm^{-1}. The reported discarded weight is negligible for all states. It is important to note that since the highest and lowest spin states for dimer **1** converge faster than the intermediate ones, a rather converged J value could also be extracted directly from the expected total span of the spin ladder. We stress however that this conclusion might not be general and that the orbitals to be used in this case still derive from a fully spin-state-averaged approach.

3.4. State-Specific Calculations and Potential Deviations from Isotropic Behavior. For comparison to the above state-averaged results, we carried out DMRG-CASSCF calculations with the same (19,16) active space but optimizing the orbitals for each spin state individually. These calculations produce the correct ordering of states, i.e. $S = 1/2$ is the ground state, but the energy intervals deviate strongly from the regular Landé pattern observed in the state-averaged calculations. The spin ladder becomes progressively compressed at higher spin levels. This effect is exaggerated at low M values and reduced significantly at higher M, but deviations remain. Compared to the state-averaged results, the two intermediate $S = 3/2$ and $S = 5/2$ states are strongly destabilized, while the high-spin $S = 7/2$ state is too low in energy: the J values computed from energy differences between adjacent levels are −74.9 cm^{-1}, −64.1 cm^{-1} and −43.8 cm^{-1}. Note that the DMRG-CASSCF total energy of each state with $M = 2000$ is already converged to within 0.2 cm^{-1} of the exact CASSCF energy. In contrast to the state-specific results obtained with the (7,10) active space, the (19,16) state-specific results follow the expected spin progression but it is still impossible to use them predictively.

This effect could go unnoticed if only two states were computed and used to extract an exchange coupling constant. One might incorrectly predict a rather optimistic value for J with DMRG-CASSCF(19,16), remaining oblivious to the fact that the complete spin ladder is inconsistent. Alternatively, results like this—when not so obviously problematic—might be treated as valid and interpreted as deviations from the isotropic bilinear HDvV Hamiltonian. Such deviations can be modeled with additional isotropic and anisotropic terms. For mixed-valence systems double exchange (coupling through an itinerant electron) may be significant, but the present system has well-localized unpaired electrons owing to the asymmetric coordination sphere that is distinct for each Mn site and of the extremely strong Jahn–Teller distortion and stabilization energy of the Mn(III) ion. These factors result in the absence of an accessible valence-interchanged state. A relevant term might instead be an

isotropic biquadratic term[149-150] of the form $-j(\mathbf{S_1S_2})^2$, which attempts to account for deviations arising from lower local M_S configurations.[130, 151-152] A previous observation that the J derived from higher spin states is weaker than that derived from lower spin states in an antiferromagnetically coupled system has been discussed in connection with biquadratic exchange.[72] In our opinion this type of analysis is in general seriously complicated by the lack of experimentally fitted j values for molecular systems, and in the present case is rendered moot by the observation that differences in J values are diminished with progressively increasing M values. Besides, the fact that J values computed even with the (19,16) active space are still far from experiment speaks against using them in deriving hypothetical extra terms. Spivak et al.[143] already described a situation where such deviations are produced as methodological artifacts (in that case of CASPT2) and additionally confirmed that previously reported deviations[72] on a Cr dimer cannot be reproduced with a state-averaged approach. Therefore, we advise caution in the use of state-specific energies in predicting deviations from isotropic Heisenberg behavior.

The divergence observed with spin state specific energies presumably arises from imbalances in the appropriateness of a given active space in recovering part of dynamic correlation or balancing ionic contributions. The energetic effect may be insignificant for many applications, but it appears sufficiently large to confound studies of exchange coupling. Based on the present observations we conclude that instead of deducing exchange coupling constants from energy differences between a limited number of isolated states, the simultaneous calculation of the complete spin ladder using averaged orbitals is to be preferred as a more robust and numerically superior approach.

3.5. Effect of Acetato Orbitals and Evaluation of Discrete Exchange Pathways. A major benefit of being able to use large active spaces with DMRG is that it provides a new powerful tool to probe the role of each diamagnetic bridge in a multiply bridged dimer, or even in systems with several paramagnetic sites and exchange pathways. Specifically, by selective inclusion of localized orbital

subspaces it is possible to switch specific exchange pathways on and off, thus quantifying the relative contribution of each bridging ligand to superexchange. Here we show how this approach can be used to compare the contribution of the oxo bridges versus the acetato ligand. There are six localized occupied orbitals on the acetato bridge; adding them to the metal-only (7,10) active space leads again to a (19,16) active space. DMRG-CASSCF calculations with this active space lead to results essentially identical to the metal-only CASSCF(7,10), with natural orbital occupation numbers of the acetato ligands remaining essentially 2.0, showing that this ligand does not contribute to superexchange.

Using both the oxo and the acetato orbitals results in an active space (31,22). DMRG-CASCI calculations up to M = 3000 with the (31,22) active space in which acetato orbitals were added to the previously optimized Mn 3d + O 2p (19,16) active space showed no appreciable deviation from the (19,16) results (J = −59.2 cm^{-1}). Orbital optimization with this larger active space was laborious but could also be completed up to M = 3000. The DMRG-CASSCF relative energies agree with the DMRG-CASCI results (Table 2), leading to an average J of −58.4 cm^{-1}. These results confirm that the acetato bridge is not mediating superexchange in this system.

The above observations are relevant for the treatment of similar systems bearing carboxylato bridges, such as the oxygen-evolving cluster of photosystem II or its many synthetic analogs. In that case the four Mn ions, which adopt combinations of oxidation states III and IV in different steps of the catalytic cycle, are connected by glutamate and aspartate residues in addition to oxo or hydroxo bridges (Figure S1). However, although the above observations in the case of dimer **1** do suggest that the acetato orbitals can be excluded, this conclusion should not be considered necessarily transferable to any system; this pathway may be deactivated in dimer **1** due to the mixed valence situation. Besides, acetato bridges are known to be magnetically active, as in the archetypal paddlewheel Cu(II) acetate dimers.[145, 153-154] Therefore, the possible roles of carboxylato bridges and concepts related to acetato ligands such as the

counter-complementarity effect are worth investigating further with a DMRG-based approach for diverse systems and metal oxidation state combinations.

Table 2. Energy level differences in cm^{-1} between spin states computed from state-averaged DMRG-CASCI and DMRG-CASSCF calculations on complex **1** with a (31,22) active space composed of Mn 3d, O 2p, and acetato orbitals for different numbers of renormalized states *M*; corresponding exchange coupling constants derived from energy differences of adjacent spin levels, and average *J* value (cm^{-1}).

	DMRG-CASCI				DMRG-CASSCF		
S	*M* = 500	*M* = 1000	*M* = 2000	*M* = 3000	*M* = 1000	*M* = 2000	*M* = 3000
7/2	791.5	862.2	880.0	882.5	841.5	869.3	870.5
5/2	469.4	474.7	476.9	477.4	467.8	470.8	471.2
3/2	249.6	200.1	184.7	182.2	202.2	180.0	179.0
1/2	0.0	0.0	0.0	0.0	0.0	0.0	0.0
$J_{(7/2–5/2)}$	-46.0	-55.4	-57.6	-57.9	-53.4	-56.9	-57.0
$J_{(5/2–3/2)}$	-44.0	-54.9	-58.4	-59.0	-53.1	-58.2	-58.4
$J_{(3/2–1/2)}$	-83.2	-66.7	-61.6	-60.7	-67.4	-60.0	-59.7
J	-57.7	-59.0	-59.2	-59.2	-58.0	-58.4	-58.4

Similarly to the above, the use of localized orbital subspaces can be used to selectively probe symmetry-distinct exchange pathways within the *same* bridging unit. For example, we performed DMRG-CASCI calculations with active spaces that included only the $2p_z$ orbitals of the O bridges in addition to the Mn 3d orbitals (π-pathway). These (11,12) active space calculations resulted in doubling the exchange coupling of the metal-only (7,10) CASSCF calculations, from −1.9 cm^{-1} to −3.9 cm^{-1}. Contrasting however this value with that of DMRG-CASCI calculations that included all O 2p orbitals in the (19,16) active space (−28.8 cm^{-1}) clearly demonstrates that the in-plane interactions between the O $2p_x/2p_y$ and the Mn $3d_{xy}$ orbitals are the dominant contributors to superexchange (σ-pathway).

Corresponding orbital transformation (COT) of broken-symmetry solutions has been used as a method to produce pairs of "magnetic orbitals" in order to visualize superexchange pathways and

quantify antiferromagnetic contributions through overlap integrals.[131] An example of COT analysis for dimer **1** is provided in Figure S2 of the Supporting Information. This method has relevance to the selective orbital subspace approach described here, because it is also a tool for investigating or mapping the "magnetic topology" of a molecular system. However, the present approach is more generally applicable because it can extend beyond two-spin systems to clusters of arbitrary nuclearity and bridging motifs, as long as appropriate orbital subspaces can be constructed and evaluated.

3.6. Effect of Virtual Orbitals. In the preceding sections we established that a spin-state-averaged DMRG-CASSCF approach with an active space encompassing all metal 3d and all oxo 2p orbitals offers a qualitatively correct description of the exchange interaction, but the result is still not quantitatively accurate. Therefore we sought to determine the possibility of improvements by inclusion of virtual orbitals in the active space. Of these the most important are the Mn 4d orbitals, which are associated with the "double shell" effect. The reason for including virtual orbitals in the active space is seen as an attempt to recover dynamic correlation.[31] We extended the previously obtained DMRG-CASSCF (19,16) optimized active orbitals with localized Mn 4d orbitals, leading to a (19,26) active space. DMRG-CASCI calculations were successful and converged at M = 3000 to a very slightly improved J value of 64.8 cm^{-1} (see Table S3) compared to the (19,16) active space. Subsequently we localized separately the oxygen 3p virtual orbitals and added them to the above (19,26) active space, leading to a final active space of 19 electrons in 32 orbitals. DMRG-CASCI(19,32) calculations with this complete set of metal 3d + 4d and oxygen 2p + 3p orbitals led to an average J value of −60.4 cm^{-1}. The maximum M that could be used for the (19,32) calculations was 1000 and still led to a spread of ca. 9 cm^{-1} ($J_{(7/2–5/2)}$ = −56.1 cm^{-1}, $J_{(5/2–3/2)}$ = −59.7 cm^{-1}, $J_{(3/2–1/2)}$ = −65.3 cm^{-1}) similar to the spread for the (19,26) results in Table S3. In analogy to the (19,26) results, we anticipate that the average would not

change significantly at higher M, so we conclude that there is no advantage in going beyond the DMRG-CASSCF(19,16) treatment within a DMRG-CASCI approach.

Orbital optimization is necessary to relax these types of excitation, but with such extended active spaces this represents a considerably more complex and computationally demanding task than calculations reported up to this point. State-averaged DMRG-CASSCF(19,26) calculations could be completed with M = 1000 and M = 1500. The results indicate that with this active space convergence of relative energies with M deteriorates dramatically. Pairwise J values evolve from $J_{(7/2–5/2)} = -39.4$ cm^{-1}, $J_{(5/2–3/2)} = -73.5$ cm^{-1}, $J_{(3/2–1/2)} = -142.3$ cm^{-1} at M = 1000 to $J_{(7/2–5/2)} = -61.3$ cm^{-1}, $J_{(5/2–3/2)} = -75.2$ cm^{-1}, $J_{(3/2–1/2)} = -97.1$ cm^{-1} at M = 1500. Obviously, even at M = 1500 the differences in pairwise J values are still too large. We note however that as shown above for the (19,16) active space (Table 1), the total span of the ladder is less sensitive to M than the relative energies of the intermediate spin levels. This is also the case for the present DMRG-CASSCF(19,26) calculations, where the relative energy of the S = 7/2 state with respect to the S = 1/2 ground state changes by less than 30 cm^{-1}, from 1070.3 cm^{-1} (M = 1000) to 1096.6 cm^{-1} (M = 1500). Using these energy differences one can derive J values of −71.4 cm^{-1} and −73.1 cm^{-1}, respectively. This implies that orbital optimization in the (19,26) active space is expected to contribute ca. 10 cm^{-1} to the magnitude of the antiferromagnetic exchange coupling compared to the CI result of Table S3. This would be an improvement over the average J obtained from the DMRG-CASSCF(19,16) calculations (Table 1). However, one is faced with the law of diminishing returns. The high cost of these calculations and the fact that quantitative accuracy is still not achieved suggests that at least in the case studied here this path is not the optimal strategy.

The approach followed up to this point treats metal and ligand orbitals as complete blocks (i.e. all metal 3d, all bridge 2p etc) and does not attempt to distinguish between more or less important ones. Attempts to select a limited number of orbitals with which to extend the minimal Anderson active space

of magnetic orbitals have been discussed in the past on a smaller scale.[51, 144] In the present work we will not diverge into the question of active space customization for the specific complex. We do expect however that this will be important for applications on exchange coupled systems that require large active spaces like the present manganese dimer. This problem is likely to be most efficiently addressed through automated screening techniques[148] based on orbital entanglement information.[155]

3.7. Perturbational Treatment of Dynamic Correlation. The importance of dynamic electron correlation for the quantitatively correct description of magnetic coupling in transition metal clusters is well established.[31] The effect of the occupied bridging orbitals is difficult to capture using dynamic electron correlation methods such as perturbation theory on top of a minimal metal-based active space[31, 156-157] and therefore is best included explicitly in the active space. On the other hand our results suggest that it might be futile to attempt to recover all dynamic electron correlation required for an accurate description of the magnetic coupling problem by aggressively extending the active space much beyond the metal d and bridge p orbitals due to the steep increase in computational cost. In contrast, dynamic electron correlation methods such as the multireference configuration interaction or canonical transformation theory for DMRG wave functions provide a computationally feasible option.[59, 158-159] Herein, we use the strongly contracted (SC) variant of NEVPT2 for DMRG to tackle dynamic electron correlation because of its robustness and good accuracy at manageable computational cost.[126, 160-162]

We examined the effect of this treatment on predicted exchange coupling constants with two of the easily accessible CAS spaces. First we applied NEVPT2 on the (7,10) active space, which had yielded an average J of −1.6 cm^{-1} by CASSCF. NEVPT2 energies lead to drastically increased antiferromagnetic coupling, with an average J of −24.8 cm^{-1} ($J_{(7/2–5/2)}$ = −22.3 cm^{-1}, $J_{(5/2–3/2)}$ = −25.2 cm^{-1}, $J_{(3/2–1/2)}$ = −26.8 cm^{-1}). Partially contracted NEVPT2 leads to a slightly better average J value of −33.6 cm^{-1}. Although NEVPT2 improves the results, quantitative agreement with experiment is not

achieved because the CASSCF reference is inadequate. The (19,16) active space that includes the Mn 3d and O 2p orbitals seems a more appropriate starting point, because it already yields a qualitatively correct description of the spin ladder at the CASSCF level.

DMRG-NEVPT2 calculations with this active space converge to an average J value of ca. −85 cm^{-1} at $M' = 1500$, which approaches the experimental value very well (Table 3). As expected, a slightly larger number of retained states is required to achieve satisfactory convergence as compared to the DMRG-CASSCF(19,16) calculations. This is due to the requirement to calculate reduced density matrices for more than two active electrons within NEVPT2.[85] With relatively small variations within the J values obtained from different steps of the spin ladder (± 0.9 cm^{-1}) we conclude that the application of NEVPT2 retains the Heisenberg behavior as it was observed for DMRG-CASSCF and CASSCF. Importantly, this finding holds true only for large M' since the different spin state energies converge at different rates with increasing M', as also described above for DMRG-CASSCF.

Table 3. Energy level differences, exchange coupling constants from adjacent spin levels and average J values (cm^{-1}) for complex **1** by DMRG-NEVPT2(19,16) calculations.

S	$M' = 500$	$M' = 1000$	$M' = 1500$
7/2	1232.2	1249.4	1268.4
5/2	668.6	674.5	676.3
3/2	262.8	259.4	256.9
1/2	0.0	0.0	0.0
$J_{(7/2–5/2)}$	-80.5	-82.1	-84.6
$J_{(5/2–3/2)}$	-81.2	-83.0	-83.9
$J_{(3/2–1/2)}$	-87.6	-86.5	-85.6
J	-83.1	-83.9	-84.7

Although the results obtained with an (19,16) active space already match the experimentally observed value within a few wavenumbers, which is on the order of the experimental accuracy, slight numerical improvement might be achieved by the inclusion of the Mn 4d orbitals in the active space thus explicitly

accounting for the "double shell effect". Considering the tight energy convergence criteria required (see above) such calculations come at immensely increased computational cost and proved to be intractable with the computer setups available to us. The present calculations already require considerable resources as the NEVPT2 algorithm requires the active space density matrices for up to four electrons, whereas regular DMRG-CASCI or DMRG-CASSCF calculations only require two-electron density matrices.[85] The formal scaling of NEVPT2 or alternative methods such as CASPT2 can in principle be reduced by application of cumulant approximations.[64, 67, 163-164] However, such approximations introduce non-negligible errors[67] and hence are inappropriate for applications to magnetic properties.

4. CONCLUSIONS AND PERSPECTIVES

DMRG holds the promise to extend the applicability of multireference methods into the field of oligonuclear magnetically coupled transition metal systems. Here we evaluated the application of DMRG to the prediction of the exchange coupling for an archetypal mixed valence manganese dimer that serves as a model for a range of materials, molecules, and bioinorganic systems. Two important conclusions of the present work are that antiferromagnetic coupling is reproduced by any choice of active space as long as orbital optimization is carried out but not otherwise, and that a spin-state-averaged approach is necessary to avoid unphysical deviations from the Landé spin ladder. Complete active space self-consistent field (CASSCF) calculations that employ a metal-only active space do not lead to reasonable values for exchange coupling constants. A physically more realistic picture of the coupled system is obtained upon inclusion of ligand-based orbitals, thus accounting for ligand-to-metal charge transfer configurations: an active space containing Mn 3d and O 2p orbitals yields an exchange coupling constant of the same order of magnitude as the experimental value, whereas the acetato bridge orbitals do not seem to have any effect. Quantitative agreement with experiment is nevertheless impossible to achieve at any readily accessible size of active space.

DMRG-NEVPT2 is used in the present study to further recover dynamic correlation. It has been suggested that perturbational treatments such as CASPT2[165] and NEVPT2 are less robust than variational methods for magnetic coupling problems.[52, 166] This is however contingent upon the quality of the starting wave function and whether the active space used is a minimal metal-based active space or not.[156-157, 167] Our results for the present dimer suggest that NEVPT2 is successful if applied to an active space comprising all metal 3d and ligand 2p orbitals. This active space represents the point where state-averaged DMRG-CASSCF already provides a qualitatively correct description of the system and pays off maximally with limited effort, whereas expanding into the virtual space entails a steep increase in complexity and cost without proportionately high returns.

At this point we would like to reflect on the applicability of the approach to larger and more complex systems. Taking the Mn_4CaO_5 cluster of the OEC as an example, the present study suggests that the smallest acceptable active space should comprise the manganese 3d and the oxo bridge 2p orbitals. This would lead to a total of 35 orbitals for the OEC,[69] which might still miss important contributions from other bridging ligands. The challenge is then how to perform a DMRG-CASSCF calculation in a state-averaged approach encompassing all necessary Heisenberg spin states. It is unclear whether such calculation is at all possible for an oligonuclear system or, alternatively, if there is a way to obtain physically realistic energy levels for a subset of the spin states without solving for the complete ladder. Most importantly, even if such calculations were possible the results are not expected to be of predictive value, while the applicability of NEVPT2 as a way to introduce meaningful corrections at such active spaces is improbable. One should also keep in mind the necessity for increasingly high M values that is exacerbated with increasing active spaces as CASSCF orbitals become progressively delocalized.

In conclusion, despite the enabling power of DMRG, quantitative results in exchange coupling constants by brute force increase of the active space are not to be expected in the near future. The

combination of full-valence DMRG-CASSCF and NEVPT2 that seems to work very well here is a pragmatic approach, but its applicability depends on the system-dependent balance of static and dynamic correlation within a given valence active space, as well as on the chemical nature of the constituent metal ions and bridging groups. In terms of defining the active space, automated orbital selection algorithms based on analysis of orbital entanglement may facilitate the selection of orbitals and help create more compact active spaces without significant loss of accuracy.[148] However we would like to caution that the orbitals eliminated in a DMRG-based prescreening are not necessarily insignificant for a subsequent NEVPT2 calculation. This topic is worth investigating more closely in the future. Instead of regarding DMRG calculations, even with very large active spaces, as a quantitative predictive tool for the analysis of exchange coupled systems it is perhaps more important and useful that one can obtain a high quality first-order description of the problem. Useful insights can be gained already at this point without quantitative accuracy, or this can form the basis for a dynamic correlation treatment. We demonstrated here one possibility, namely NEVPT2, but other approaches can be considered[159, 168-171] and will be investigated in future work.

Supporting Information. Additional figures and results. This material is available free of charge via the Internet at http://pubs.acs.org.

Corresponding Authors

* Email: michael.roemelt@theochem.rub.de, v.krewald@bath.ac.uk, dimitrios.pantazis@cec.mpg.de

ACKNOWLEDGMENT

The Max Planck Society is gratefully acknowledged for funding. M.R. would like to gratefully acknowledge funding by the “Otto-Hahn” program of the Max-Planck Society. V.K. is grateful for funding and support through a 50th Anniversary Prize Fellowship of the University of Bath. D.A.P. acknowledges support by the project MANGAN (03EK3545) funded by the Bundesministeriums für

Bildung und Forschung (BMBF). V.K. and D.A.P. acknowledge network support by the COST action CM1305 “Explicit Control Over Spin-states in Technology and Biochemistry” (ECOSTBio).

REFERENCES

1. Ceulemans, A.; Chibotaru, L. F.; Heylen, G. A.; Pierloot, K.; Vanquickenborne, L. G. Theoretical Models of Exchange Interactions in Dimeric Transition-Metal Complexes. *Chem. Rev.* **2000,** *100*, 787-806.

2. Thompson, L. K.; Waldmann, O.; Xu, Z. Polynuclear manganese grids and clusters–A magnetic perspective. *Coord. Chem. Rev.* **2005,** *249*, 2677-2690.

3. Ruiz, E. Theoretical study of the exchange coupling in large polynuclear transition metal complexes using DFT methods. *Struct. Bonding* **2004,** *113*, 91-102.

4. Moreira, I. d. P. R.; Illas, F. A unified view of the theoretical description of magnetic coupling in molecular chemistry and solid state physics. *Phys. Chem. Chem. Phys.* **2006,** *8*, 1645-1659.

5. Rudberg, E.; Sałek, P.; Rinkevicius, Z.; Ågren, H. Heisenberg Exchange in Dinuclear Manganese Complexes: A Density Functional Theory Study. *J. Chem. Theory Comput.* **2006,** *2*, 981-989.

6. Bagai, R.; Christou, G. The Drosophila of single-molecule magnetism: $[Mn_{12}O_{12}(O_2CR)_{16}(H_2O)_4]$. *Chem. Soc. Rev.* **2009,** *38*, 1011-1026.

7. Glaser, T. Rational design of single-molecule magnets: a supramolecular approach. *Chem. Commun.* **2011,** *47*, 116-130.

8. Murrie, M. Cobalt(II) single-molecule magnets. *Chem. Soc. Rev.* **2010,** *39*, 1986-1995.

9. Yang, C.-I.; Zhang, Z.-Z.; Lin, S.-B. A review of manganese-based molecular magnets and supramolecular architectures from phenolic oximes. *Coord. Chem. Rev.* **2015,** *289-290*, 289-314.

10. Mukhopadhyay, S.; Mandal, S. K.; Bhaduri, S.; Armstrong, W. H. Manganese clusters with relevance to photosystem II. *Chem. Rev.* **2004,** *104*, 3981-4026.

11. Gerey, B.; Gouré, E.; Fortage, J.; Pécaut, J.; Collomb, M.-N. Manganese-calcium/strontium heterometallic compounds and their relevance for the oxygen-evolving center of photosystem II. *Coord. Chem. Rev.* **2016,** *319*, 1-24.

12. Paul, S.; Neese, F.; Pantazis, D. A. Structural models of the biological oxygen-evolving complex: achievements, insights, and challenges for biomimicry. *Green Chem.* **2017,** *19*, 2309-2325.

13. Mukherjee, S.; Stull, J. A.; Yano, J.; Stamatatos, T. C.; Pringouri, K.; Stich, T. A.; Abboud, K. A.; Britt, R. D.; Yachandra, V. K.; Christou, G. Synthetic model of the asymmetric $[Mn_3CaO_4]$ cubane core of the oxygen-evolving complex of photosystem II. *Proc. Natl. Acad. Sci. U.S.A.* **2012,** *109*, 2257-2262.

14. Krewald, V.; Neese, F.; Pantazis, D. A. On the magnetic and spectroscopic properties of high-valent Mn_3CaO_4 cubanes as structural units of natural and artificial water oxidizing catalysts. *J. Am. Chem. Soc.* **2013,** *135*, 5726-5739.

15. Zhang, C.; Chen, C.; Dong, H.; Shen, J.-R.; Dau, H.; Zhao, J. A synthetic Mn_4Ca-cluster mimicking the oxygen-evolving center of photosynthesis. *Science* **2015,** *348*, 690-693.

16. Kanady, J. S.; Tsui, E. Y.; Day, M. W.; Agapie, T. A Synthetic Model of the Mn_3Ca Subsite of the Oxygen-Evolving Complex in Photosystem II. *Science* **2011,** *333*, 733-736.

17. Noodleman, L. Valence bond description of anti-ferromagnetic coupling in transition-metal dimers. *J. Chem. Phys.* **1981,** *74*, 5737-5743.

18. Noodleman, L.; Davidson, E. R. Ligand spin polarization and antiferromagnetic coupling in transition-metal dimers. *Chem. Phys.* **1986,** *109*, 131-143.

19. Noodleman, L.; Case, D. A. Density-Functional Theory of Spin Polarization and Spin Coupling in Iron-Sulfur Clusters. *Adv. Inorg. Chem.* **1992,** *38*, 423-470.

20. Noodleman, L.; Peng, C. Y.; Case, D. A.; Mouesca, J. M. Orbital Interactions, Electron Delocalization and Spin Coupling in Iron-Sulfur Clusters. *Coord. Chem. Rev.* **1995,** *144*, 199-244.

21. Yamaguchi, K.; Tsunekawa, T.; Toyoda, Y.; Fueno, T. Ab initio molecular orbital calculations of effective exchange integrals between transition metal ions. *Chem. Phys. Lett.* **1988,** *143*, 371-376.

22. Yamanaka, S.; Kawakami, T.; Nagao, H.; Yamaguchi, K. Effective exchange integrals for open-shell species by density functional methods. *Chem. Phys. Lett.* **1994,** *231*, 25-33.

23. Bencini, A.; Totti, F.; Daul, C. A.; Doclo, K.; Fantucci, P.; Barone, V. Density Functional Calculations of Magnetic Exchange Interactions in Polynuclear Transition Metal Complexes. *Inorg. Chem.* **1997,** *36*, 5022-5030.

24. Nagao, H.; Nishino, M.; Shigeta, Y.; Soda, T.; Kitagawa, Y.; Onishi, T.; Yoshioka, Y.; Yamaguchi, K. Theoretical studies on effective spin interactions, spin alignments and macroscopic spin tunneling in polynuclear manganese and related complexes and their mesoscopic clusters. *Coord. Chem. Rev.* **2000,** *198*, 265-295.

25. Ruiz, E.; Rodriguez-Fortea, A.; Cano, J.; Alvarez, S.; Alemany, P. About the calculation of exchange coupling constants in polynuclear transition metal complexes. *J. Comput. Chem.* **2003,** *24*, 982-989.

26. Shoji, M.; Koizumi, K.; Kitagawa, Y.; Kawakami, T.; Yamanaka, S.; Okumura, M.; Yamaguchi, K. A general algorithm for calculation of Heisenberg exchange integrals *J* in multispin systems. *Chem. Phys. Lett.* **2006,** *432*, 343-347.

27. Neese, F. Prediction of molecular properties and molecular spectroscopy with density functional theory: From fundamental theory to exchange-coupling. *Coord. Chem. Rev.* **2009,** *253*, 526-563.

28. Bencini, A.; Totti, F. A Few Comments on the Application of Density Functional Theory to the Calculation of the Magnetic Structure of Oligo-Nuclear Transition Metal Clusters. *J. Chem. Theory Comput.* **2009,** *5*, 144-154.

29. Cirera, J.; Ruiz, E., Modeling Magnetic Properties with Density Functional Theory-Based Methods. In *Molecular Magnetic Materials*, Sieklucka, B.; Pinkowicz, D., Eds. Wiley-VCH: 2017; pp 419-446.

30. Ciofini, I.; Daul, C. A. DFT calculations of molecular magnetic properties of coordination compounds. *Coord. Chem. Rev.* **2003,** *238-239*, 187-209.

31. Malrieu, J. P.; Caballol, R.; Calzado, C. J.; de Graaf, C.; Guihery, N. Magnetic interactions in molecules and highly correlated materials: physical content, analytical derivation, and rigorous extraction of magnetic Hamiltonians. *Chem. Rev.* **2014,** *114*, 429-92.

32. Caballol, R.; Castell, O.; Illas, F.; de P. R. Moreira, I.; Malrieu, J. P. Remarks on the Proper Use of the Broken Symmetry Approach to Magnetic Coupling. *J. Phys. Chem. A* **1997,** *101*, 7860-7866.

33. Pantazis, D. A.; Orio, M.; Petrenko, T.; Zein, S.; Bill, E.; Lubitz, W.; Messinger, J.; Neese, F. A new quantum chemical approach to the magnetic properties of oligonuclear transition-metal complexes: Application to a model for the tetranuclear manganese cluster of Photosystem II. *Chem.—Eur. J.* **2009,** *15*, 5108-5123.

34. Illas, F.; Moreira, I. P. R.; de Graaf, C.; Barone, V. Magnetic coupling in biradicals, binuclear complexes and wide-gap insulators: a survey of ab initio wave function and density functional theory approaches. *Theor. Chem. Acc.* **2000,** *104*, 265-272.

35. Illas, F.; Moreira, I. d. P. R.; Bofill, J. M.; Filatov, M. Spin Symmetry Requirements in Density Functional Theory: The Proper Way to Predict Magnetic Coupling Constants in Molecules and Solids. *Theor. Chem. Acc.* **2006,** *116*, 587-597.

36. Illas, F.; de P. R. Moreira, I.; Bofill, J. M.; Filatov, M. Extent and limitations of density-functional theory in describing magnetic systems. *Phys. Rev. B* **2004,** *70*, 132414.

37. Zein, S.; Poor Kalhor, M.; Chibotaru, L. F.; Chermette, H. Density functional estimations of Heisenberg exchange constants in oligonuclear magnetic compounds: Assessment of density functional theory versus ab initio. *J. Chem. Phys.* **2009,** *131*, 224316.

38. Luo, S.; Rivalta, I.; Batista, V.; Truhlar, D. G. Noncollinear Spins Provide a Self-Consistent Treatment of the Low-Spin State of a Biomimetic Oxomanganese Synthetic Trimer Inspired by the Oxygen Evolving Complex of Photosystem II. *J. Phys. Chem. Lett.* **2011,** *2*, 2629-2633.

39. Phillips, J. J.; Peralta, J. E. Towards the blackbox computation of magnetic exchange coupling parameters in polynuclear transition-metal complexes: Theory, implementation, and application. *J. Chem. Phys.* **2013,** *138*, 174115.

40. Phillips, J. J.; Peralta, J. E.; Christou, G. Magnetic Couplings in Spin Frustrated Fe_7^{III} Disklike Clusters. *J. Chem. Theory Comput.* **2013,** *9*, 5585-5589.

41. Steenbock, T.; Tasche, J.; Lichtenstein, A. I.; Herrmann, C. A Green's-Function Approach to Exchange Spin Coupling As a New Tool for Quantum Chemistry. *J. Chem. Theory Comput.* **2015,** *11*, 5651-5664.

42. Peralta, J. E.; Barone, V. Magnetic exchange couplings from noncollinear spin density functional perturbation theory. *J. Chem. Phys.* **2008,** *129*, 194107.

43. Zhekova, H.; Seth, M.; Ziegler, T. Introduction of a New Theory for the Calculation of Magnetic Coupling Based on Spin-Flip Constricted Variational Density Functional Theory. Application to Trinuclear Copper Complexes which Model the Native Intermediate in Multicopper Oxidases. *J. Chem. Theory Comput.* **2011,** *7*, 1858-1866.

44. Valero, R.; Illas, F.; Truhlar, D. G. Magnetic Coupling in Transition-Metal Binuclear Complexes by Spin-Flip Time-Dependent Density Functional Theory. *J. Chem. Theory Comput.* **2011,** *7*, 3523-3531.

45. Szalay, P. G.; Müller, T.; Gidofalvi, G.; Lischka, H.; Shepard, R. Multiconfiguration Self-Consistent Field and Multireference Configuration Interaction Methods and Applications. *Chem. Rev.* **2012,** *112*, 108-181.

46. Miralles, J.; Daudey, J.-P.; Caballol, R. Variational calculation of small energy differences. The singlet-triplet gap in $[Cu_2Cl_6]^{2-}$. *Chem. Phys. Lett.* **1992,** *198*, 555-562.

47. Miralles, J.; Castell, O.; Caballol, R.; Malrieu, J.-P. Specific CI calculation of energy differences: Transition energies and bond energies. *Chem. Phys.* **1993,** *172*, 33-43.

48. Castell, O.; Caballol, R. Ab Initio Configuration Interaction Calculation of the Exchange Coupling Constant in Hydroxo Doubly Bridged Cr(III) Dimers. *Inorg. Chem.* **1999,** *38*, 668-673.

49. Calzado, C. J.; Cabrero, J.; Malrieu, J. P.; Caballol, R. Analysis of the magnetic coupling in binuclear complexes. I. Physics of the coupling. *J. Chem. Phys.* **2002,** *116*, 2728-2747.

50. Calzado, C. J.; Cabrero, J.; Malrieu, J. P.; Caballol, R. Analysis of the magnetic coupling in binuclear complexes. II. Derivation of valence effective Hamiltonians from ab initio CI and DFT calculations. *J. Chem. Phys.* **2002,** *116*, 3985-4000.

51. Calzado, C. J.; Angeli, C.; Caballol, R.; Malrieu, J.-P. Extending the active space in multireference configuration interaction calculations of magnetic coupling constants. *Theor. Chem. Acc.* **2010,** *126*, 185-196.

52. Calzado, C. J.; Angeli, C.; Taratiel, D.; Caballol, R.; Malrieu, J. P. Analysis of the magnetic coupling in binuclear systems. III. The role of the ligand to metal charge transfer excitations revisited. *J. Chem. Phys.* **2009,** *131*, 044327.

53. White, S. R. Density matrix formulation for quantum renormalization groups. *Phys. Rev. Lett.* **1992,** *69*, 2863-2866.

54. White, S. R.; Martin, R. L. Ab initio quantum chemistry using the density matrix renormalization group. *J. Chem. Phys.* **1999,** *110*, 4127-4130.

55. Chan, G. K.-L.; Sharma, S. The density matrix renormalization group in quantum chemistry. *Annu. Rev. Phys. Chem.* **2011,** *62*, 465-481.

56. Marti, K. H.; Reiher, M. New electron correlation theories for transition metal chemistry. *Phys. Chem. Chem. Phys.* **2011,** *13*, 6750-6759.

57. Schollwöck, U. The density-matrix renormalization group in the age of matrix product states. *Ann. Phys.* **2011,** *326*, 96-192.

58. Keller, S. F.; Reiher, M. Determining Factors for the Accuracy of DMRG in Chemistry. *Chimia* **2014,** *68*, 200-203.

59. Saitow, M.; Kurashige, Y.; Yanai, T. Fully Internally Contracted Multireference Configuration Interaction Theory Using Density Matrix Renormalization Group: A Reduced-Scaling Implementation Derived by Computer-Aided Tensor Factorization. *J. Chem. Theory Comput.* **2015,** *11*, 5120-5131.

60. Zgid, D.; Nooijen, M. The density matrix renormalization group self-consistent field method: Orbital optimization with the density matrix renormalization group method in the active space. *J. Chem. Phys.* **2008,** *128*, 144116.

61. Zgid, D.; Nooijen, M. Obtaining the two-body density matrix in the density matrix renormalization group method. *J. Chem. Phys.* **2008,** *128*, 144115.

62. Marti, K. H.; Ondík, I. M.; Moritz, G.; Reiher, M. Density matrix renormalization group calculations on relative energies of transition metal complexes and clusters. *J. Chem. Phys.* **2008,** *128*, 014104.

63. Kurashige, Y.; Yanai, T. High-performance ab initio density matrix renormalization group method: Applicability to large-scale multireference problems for metal compounds. *J. Chem. Phys.* **2009,** *130*, 234114.

64. Kurashige, Y.; Chalupský, J.; Lan, T. N.; Yanai, T. Complete active space second-order perturbation theory with cumulant approximation for extended active-space wavefunction from density matrix renormalization group. *J. Chem. Phys.* **2014,** *141*, 174111.

65. Kurashige, Y.; Saitow, M.; Chalupsky, J.; Yanai, T. Radical O-O coupling reaction in diferrate-mediated water oxidation studied using multireference wave function theory. *Phys. Chem. Chem. Phys.* **2014,** *16*, 11988-11999.

66. Freitag, L.; Knecht, S.; Keller, S. F.; Delcey, M. G.; Aquilante, F.; Pedersen, T. B.; Lindh, R.; Reiher, M.; Gonzalez, L. Orbital entanglement and CASSCF analysis of the Ru-NO bond in a Ruthenium nitrosyl complex. *Phys. Chem. Chem. Phys.* **2015,** *17*, 14383-14392.

67. Phung, Q. M.; Wouters, S.; Pierloot, K. Cumulant Approximated Second-Order Perturbation Theory Based on the Density Matrix Renormalization Group for Transition Metal Complexes: A Benchmark Study. *J. Chem. Theory Comput.* **2016,** *12*, 4352-4361.

68. Nakatani, N.; Guo, S. Density matrix renormalization group (DMRG) method as a common tool for large active-space CASSCF/CASPT2 calculations. *J. Chem. Phys.* **2017,** *146*, 094102.

69. Kurashige, Y.; Chan, G. K.-L.; Yanai, T. Entangled quantum electronic wavefunctions of the Mn_4CaO_5 cluster in photosystem II. *Nat. Chem.* **2013,** *5*, 660-666.

70. Paul, S.; Cox, N.; Pantazis, D. A. What can we learn from a biomimetic model of nature's oxygen-evolving complex? *Inorg. Chem.* **2017,** *56*, 3875-3888.

71. Sharma, S.; Sivalingam, K.; Neese, F.; Chan, G. K.-L. Low-energy spectrum of iron–sulfur clusters directly from many-particle quantum mechanics. *Nat. Chem.* **2014,** *6*, 927-933.

72. Harris, T. V.; Kurashige, Y.; Yanai, T.; Morokuma, K. Ab initio density matrix renormalization group study of magnetic coupling in dinuclear iron and chromium complexes. *J. Chem. Phys.* **2014,** *140*, 054303.

73. Bossek, U.; Saher, M.; Weyhermuller, T.; Wieghardt, K. Asymmetric mixed valence manganese complexes containing the $[Mn(\mu\text{-}O)_2(\mu\text{-}MeCo_2)Mn]^{2+}$ core and their catalase reactivity. *J. Chem. Soc., Chem. Commun.* **1992**, 1780-1782.

74. McGrady, J. E.; Stranger, R. Redox-induced changes in the geometry and electronic structure of di-μ-oxo-bridged manganese dimers. *J. Am. Chem. Soc.* **1997,** *119*, 8512-8522.

75. Petrie, S.; Mukhopadhyay, S.; Armstrong, W. H.; Stranger, R. Theoretical analysis of the $[Mn_2(\mu\text{-}oxo)_2(\mu\text{-}carboxylato)_2]^+$ core. *Phys. Chem. Chem. Phys.* **2004,** *6*, 4871-4877.

76. Orio, M.; Pantazis, D. A.; Petrenko, T.; Neese, F. Magnetic and Spectroscopic Properties of Mixed Valence Manganese(III,IV) Dimers: A Systematic Study Using Broken Symmetry Density Functional Theory. *Inorg. Chem.* **2009,** *48*, 7251-7260.

77. Baffert, C.; Orio, M.; Pantazis, D. A.; Duboc, C.; Blackman, A. G.; Blondin, G.; Neese, F.; Deronzier, A.; Collomb, M.-N. Trinuclear Terpyridine Frustrated Spin System with a $Mn^{IV}{}_3O_4$ Core: Synthesis, Physical Characterization, and Quantum Chemical Modeling of Its Magnetic Properties. *Inorg. Chem.* **2009,** *48*, 10281-10288.

78. Fliegl, H.; Fink, K.; Klopper, W.; Anson, C. E.; Powell, A. K.; Clerac, R. Ab initio study of the magnetic exchange coupling constants of a structural model $[CaMn_3{}^{III}Mn^{II}]$ of the oxygen evolving center in photosystem II. *Phys. Chem. Chem. Phys.* **2009,** *11*, 3900-3909.

79. Schinzel, S.; Kaupp, M. Validation of broken-symmetry density functional methods for the calculation of electron paramagnetic resonance parameters of dinuclear mixed-valence $Mn^{IV}Mn^{III}$ complexes. *Can. J. Chem.* **2009,** *87*, 1521-1539.

80. Vogiatzis, K. D.; Klopper, W.; Mavrandonakis, A.; Fink, K. Magnetic properties of paddlewheels and trinuclear clusters with exposed metal sites. *ChemPhysChem* **2011,** *12*, 3307-3319.

81. Pantazis, D. A.; Krewald, V.; Orio, M.; Neese, F. Theoretical magnetochemistry of dinuclear manganese complexes: broken symmetry density functional theory investigation on the influence of bridging motifs on structure and magnetism. *Dalton Trans.* **2010,** *39*, 4959-4967.

82. Bovi, D.; Guidoni, L. Magnetic coupling constants and vibrational frequencies by extended broken symmetry approach with hybrid functionals. *J. Chem. Phys.* **2012,** *137*, 114107.

83. Shoji, M.; Isobe, H.; Shen, J. R.; Yamaguchi, K. Geometric and electronic structures of the synthetic Mn_4CaO_4 model compound mimicking the photosynthetic oxygen-evolving complex. *Phys. Chem. Chem. Phys.* **2016,** *18*, 11330-11340.

84. Angeli, C.; Cimiraglia, R.; Evangelisti, S.; Leininger, T.; Malrieu, J. P. Introduction of n-electron valence states for multireference perturbation theory. *J. Chem. Phys.* **2001,** *114*, 10252-10264.

85. Angeli, C.; Cimiraglia, R.; Malrieu, J.-P. n-electron valence state perturbation theory: A spinless formulation and an efficient implementation of the strongly contracted and of the partially contracted variants. *J. Chem. Phys.* **2002,** *117*, 9138-9153.

86. Krewald, V.; Retegan, M.; Pantazis, D. A. Principles of Natural Photosynthesis. *Top. Curr. Chem.* **2016,** *371*, 23-48.

87. Siegbahn, P. E. M. Water oxidation mechanism in photosystem II, including oxidations, proton release pathways, O–O bond formation and O_2 release. *Biochim. Biophys. Acta Bioenerg.* **2013,** *1827*, 1003-1019.

88. Cox, N.; Pantazis, D. A.; Neese, F.; Lubitz, W. Biological water oxidation. *Acc. Chem. Res.* **2013,** *46*, 1588-1596.

89. Krewald, V.; Retegan, M.; Cox, N.; Messinger, J.; Lubitz, W.; DeBeer, S.; Neese, F.; Pantazis, D. A. Metal oxidation states in biological water splitting. *Chem. Sci.* **2015,** *6*, 1676-1695.

90. Askerka, M.; Brudvig, G. W.; Batista, V. S. The O2-Evolving Complex of Photosystem II: Recent Insights from Quantum Mechanics/Molecular Mechanics (QM/MM), Extended X-ray Absorption Fine Structure (EXAFS), and Femtosecond X-ray Crystallography Data. *Acc. Chem. Res.* **2017,** *50*, 41-48.

91. Dau, H.; Haumann, M. The manganese complex of photosystem II in its reaction cycle–Basic framework and possible realization at the atomic level. *Coord. Chem. Rev.* **2008,** *252*, 273-295.

92. Klauss, A.; Haumann, M.; Dau, H. Alternating electron and proton transfer steps in photosynthetic water oxidation. *Proc. Natl. Acad. Sci. U.S.A.* **2012,** *109*, 16035-16040.

93. Pantazis, D. A.; Ames, W.; Cox, N.; Lubitz, W.; Neese, F. Two interconvertible structures that explain the spectroscopic properties of the oxygen-evolving complex of photosystem II in the S_2 state. *Angew. Chem., Int. Ed.* **2012,** *51*, 9935-9940.

94. Yamaguchi, K.; Yamanaka, S.; Isobe, H.; Saito, T.; Kanda, K.; Umena, Y.; Kawakami, K.; Shen, J. R.; Kamiya, N.; Okumura, M.; Nakamura, H.; Shoji, M.; Yoshioka, Y. The nature of chemical bonds of the $CaMn_4O_5$ cluster in oxygen evolving complex of photosystem II: Jahn-Teller distortion and its suppression by Ca doping in cubane structures. *Int. J. Quantum Chem.* **2013,** *113*, 453-473.

95. Suga, M.; Akita, F.; Hirata, K.; Ueno, G.; Murakami, H.; Nakajima, Y.; Shimizu, T.; Yamashita, K.; Yamamoto, M.; Ago, H.; Shen, J.-R. Native structure of photosystem II at 1.95 Å resolution viewed by femtosecond X-ray pulses. *Nature* **2015,** *517*, 99-103.

96. Ferreira, K. N.; Iverson, T. M.; Maghlaoui, K.; Barber, J.; Iwata, S. Architecture of the photosynthetic oxygen-evolving center. *Science* **2004,** *303*, 1831-1838.

97. Umena, Y.; Kawakami, K.; Shen, J.-R.; Kamiya, N. Crystal structure of the oxygen-evolving photosystem II at a resolution of 1.9 Å. *Nature* **2011,** *473*, 55-60.

98. Neese, F. The ORCA program system. *WIREs Comput. Mol. Sci.* **2012,** *2*, 73-78.

99. Chan, G. K.-L.; Head-Gordon, M. Highly correlated calculations with a polynomial cost algorithm: A study of the density matrix renormalization group. *J. Chem. Phys.* **2002,** *116*, 4462-4476.

100. Chan, G. K.-L. An algorithm for large scale density matrix renormalization group calculations. *J. Chem. Phys.* **2004,** *120*, 3172-3178.

101. Ghosh, D.; Hachmann, J.; Yanai, T.; Chan, G. K.-L. Orbital optimization in the density matrix renormalization group, with applications to polyenes and β-carotene. *J. Chem. Phys.* **2008,** *128*, 144117.

102. Sharma, S.; Chan, G. K.-L. Spin-adapted density matrix renormalization group algorithms for quantum chemistry. *J. Chem. Phys.* **2012,** *136*, 124121.

103. Tao, J.; Perdew, J. P.; Staroverov, V. N.; Scuseria, G. E. Climbing the Density Functional Ladder: Nonempirical Meta-Generalized Gradient Approximation Designed for Molecules and Solids. *Phys. Rev. Lett.* **2003,** *91*, 146401.

104. Grimme, S.; Antony, J.; Ehrlich, S.; Krieg, H. A consistent and accurate ab initio parametrization of density functional dispersion correction (DFT-D) for the 94 elements H–Pu. *J. Chem. Phys.* **2010,** *132*, 154104.

105. Grimme, S.; Ehrlich, S.; Goerigk, L. Effect of the damping function in dispersion corrected density functional theory. *J. Comput. Chem.* **2011,** *32*, 1456-1465.

106. Staroverov, V. N.; Scuseria, G. E.; Tao, J.; Perdew, J. P. Comparative assessment of a new nonempirical density functional: Molecules and hydrogen-bonded complexes. *J. Chem. Phys.* **2003,** *119*, 12129-12137.

107. Perdew, J. P. Density-functional approximation for the correlation-energy of the inhomogeneous electron-gas. *Phys. Rev. B* **1986,** *33*, 8822-8824.

108. Becke, A. D. Density-functional exchange-energy approximation with correct asymptotic-behavior. *Phys. Rev. A* **1988,** *38*, 3098-3100.

109. Zhao, Y.; Truhlar, D. G. The M06 suite of density functionals for main group thermochemistry, thermochemical kinetics, noncovalent interactions, excited states, and transition elements: two new functionals and systematic testing of four M06-class functionals and 12 other functionals. *Theor. Chem. Acc.* **2008,** *120*, 215-241.

110. van Lenthe, E.; Baerends, E. J.; Snijders, J. G. Relativistic regular two-component Hamiltonians. *J. Chem. Phys.* **1993,** *99*, 4597-4610.

111. van Leeuwen, R.; van Lenthe, E.; Baerends, E. J.; Snijders, J. G. Exact solutions of regular approximate relativistic wave equations for hydrogen- like atoms. *J. Chem. Phys.* **1994,** *101*, 1272-1281.

112. van Lenthe, E.; Baerends, E. J.; Snijders, J. G. Relativistic total-energy using regular approximations. *J. Chem. Phys.* **1994,** *101*, 9783-9792.

113. van Wüllen, C. Molecular density functional calculations in the regular relativistic approximation: Method, application to coinage metal diatomics, hydrides, fluorides and chlorides, and comparison with first-order relativistic calculations *J. Chem. Phys.* **1998,** *109*, 392-399.

114. Filatov, M.; Cremer, D. On the physical meaning of the ZORA Hamiltonian. *Mol. Phys.* **2003,** *101*, 2295-2302.

115. Pantazis, D. A.; Chen, X. Y.; Landis, C. R.; Neese, F. All-electron scalar relativistic basis sets for third-row transition metal atoms. *J. Chem. Theory Comput.* **2008,** *4*, 908-919.

116. Weigend, F.; Ahlrichs, R. Balanced basis sets of split valence, triple zeta valence and quadruple zeta valence quality for H to Rn: Design and assessment of accuracy. *Phys. Chem. Chem. Phys.* **2005,** *7*, 3297-3305.

117. Weigend, F. Accurate Coulomb-fitting basis sets for H to Rn. *Phys. Chem. Chem. Phys.* **2006,** *8*, 1057-1065.

118. Hattig, C. Optimization of auxiliary basis sets for RI-MP2 and RI-CC2 calculations: Core-valence and quintuple-zeta basis sets for H to Ar and QZVPP basis sets for Li to Kr. *Phys. Chem. Chem. Phys.* **2005,** *7*, 59-66.

119. Pipek, J.; Mezey, P. G. A fast intrinsic localization procedure applicable for ab initio and semiempirical linear combination of atomic orbital wave functions. *J. Chem. Phys.* **1989,** *90*, 4916-4926.

120. Neese, F. Importance of Direct Spin-Spin Coupling and Spin-Flip Excitations for the Zero-Field Splittings of Transition Metal Complexes: A Case Study. *J. Am. Chem. Soc.* **2006,** *128*, 10213-10222.

121. Fiedler, M. A property of eigenvectors of nonnegative symmetric matrices and its application to graph theory. *Czech. Math. J.* **1975,** *25*, 619-633.

122. Fiedler, M. Algebraic connectivity of graphs. *Czech. Math. J.* **1973,** *23*, 298-305.

123. Atkins, J. E.; Boman, E. G.; Hendrickson, B. A Spectral Algorithm for Seriation and the Consecutive Ones Problem. *SIAM J. Comput.* **1998,** *28*, 297-310.

124. Barcza, G.; Legeza, Ö.; Marti, K. H.; Reiher, M. Quantum-information analysis of electronic states of different molecular structures. *Phys. Rev. A* **2011,** *83*, 012508.

125. McLean, A. D.; Liu, B. Classification of configurations and the determination of interacting and noninteracting spaces in configuration interaction. *J. Chem. Phys.* **1973,** *58*, 1066-1078.

126. Guo, S.; Watson, M. A.; Hu, W.; Sun, Q.; Chan, G. K.-L. *N*-Electron Valence State Perturbation Theory Based on a Density Matrix Renormalization Group Reference Function, with Applications to the Chromium Dimer and a Trimer Model of Poly(p-Phenylenevinylene). *J. Chem. Theory Comput.* **2016,** *12*, 1583-1591.

127. Olivares-Amaya, R.; Hu, W.; Nakatani, N.; Sharma, S.; Yang, J.; Chan, G. K.-L. The ab-initio density matrix renormalization group in practice. *J. Chem. Phys.* **2015,** *142*, 034102.

128. Kahn, O. *Molecular Magnetism*. Wiley VCH: New York, 1993; p 396.

129. Mabbs, F. E.; Machin, D. J. *Magnetism and transition metal complexes*. Chapman & Hall: London, 1973; p 240.

130. Bastardis, R.; Guihery, N.; de Graaf, C. Isotropic non-Heisenberg terms in the magnetic coupling of transition metal complexes. *J. Chem. Phys.* **2008,** *129*, 104102.

131. Neese, F. Definition of corresponding orbitals and the diradical character in broken symmetry DFT calculations on spin coupled systems. *J. Phys. Chem. Solids* **2004,** *65*, 781-785.

132. Zhao, X. G.; Richardson, W. H.; Chen, J. L.; Li, J.; Noodleman, L.; Tsai, H. L.; Hendrickson, D. N. Density Functional Calculations of Electronic Structure, Charge Distribution, and Spin Coupling in Manganese-Oxo Dimer Complexes. *Inorg. Chem.* **1997,** *36*, 1198-1217.

133. Ruiz, E.; Cano, J.; Alvarez, S.; Alemany, P. Broken symmetry approach to calculation of exchange coupling constants for homobinuclear and heterobinuclear transition metal complexes. *J. Comput. Chem.* **1999,** *20*, 1391-1400.

134. Yamaguchi, K.; Takahara, Y.; Fueno, T., Ab-Initio Molecular Orbital Studies of Structure and Reactivity of Transition Metal-Oxo Compounds. In *Applied Quantum Chemistry*, Smith Jr., V. H.; Scheafer III, H. F.; Morokuma, K., Eds. D. Reidel: Boston, 1986; pp 155-184.

135. Kanda, K.; Yamanaka, S.; Saito, T.; Umena, Y.; Kawakami, K.; Shen, J.-R.; Kamiya, N.; Okumura, M.; Nakamura, H.; Yamaguchi, K. Labile electronic and spin states of the $CaMn_4O_5$ cluster in the PSII system refined to the 1.9 Å X-ray resolution. UB3LYP computational results. *Chem. Phys. Lett.* **2011,** *506*, 98-103.

136. Sameera, W. M. C.; Piñero, D. M.; Herchel, R.; Sanakis, Y.; McGrady, J. E.; Raptis, R. G.; Zueva, E. M. A Combined Experimental and Computational Study of the Magnetic Superexchange within a Triangular (μ_3-O)-Pyrazolato-Fe^{III}_3 Complex. *Eur. J. Inorg. Chem.* **2012,** *2012*, 3500-3506.

137. Zueva, E. M.; Herchel, R.; Borshch, S. A.; Govor, E. V.; Sameera, W. M. C.; McDonald, R.; Singleton, J.; Krzystek, J.; Travnicek, Z.; Sanakis, Y.; McGrady, J. E.; Raptis, R. G. Double exchange in a mixed-valent octanuclear iron cluster, $[Fe_8(\mu_4\text{-}O)_4(\mu\text{-}4\text{-}Cl\text{-}pz)_{12}Cl_4]^-$. *Dalton Trans.* **2014,** *43*, 11269-11276.

138. Yamaguchi, K.; Isobe, H.; Shoji, M.; Yamanaka, S.; Okumura, M. Theory of chemical bonds in metalloenzymes XX: magneto-structural correlations in the $CaMn_4O_5$ cluster in oxygen-evolving complex of photosystem II. *Mol. Phys.* **2015**, 1-28.

139. Isobe, H.; Shoji, M.; Yamanaka, S.; Mino, H.; Umena, Y.; Kawakami, K.; Kamiya, N.; Shen, J. R.; Yamaguchi, K. Generalized approximate spin projection calculations of effective exchange integrals of the $CaMn_4O_5$ cluster in the S_1 and S_3 states of the oxygen evolving complex of photosystem II. *Phys. Chem. Chem. Phys.* **2014,** *16*, 11911-11923.

140. Foster, J. M.; Boys, S. F. Canonical Configurational Interaction Procedure. *Rev. Mod. Phys.* **1960,** *32*, 300-302.

141. Cabrero, J.; Calzado, C. J.; Maynau, D.; Caballol, R.; Malrieu, J. P. Metal–Ligand Delocalization in Magnetic Orbitals of Binuclear Complexes. *J. Phys. Chem. A* **2002,** *106*, 8146-8155.

142. Angeli, C.; Calzado, C. J. The role of the magnetic orbitals in the calculation of the magnetic coupling constants from multireference perturbation theory methods. *J. Chem. Phys.* **2012,** *137*, 034104.

143. Spivak, M.; Angeli, C.; Calzado, C. J.; de Graaf, C. Improving the calculation of magnetic coupling constants in MRPT methods. *J. Comput. Chem.* **2014,** *35*, 1665-1671.

144. Bordas, E.; Caballol, R.; de Graaf, C.; Malrieu, J.-P. Toward a variational treatment of the magnetic coupling between centers with elevated spin moments. *Chem. Phys.* **2005,** *309*, 259-269.

145. De Loth, P.; Cassoux, P.; Daudey, J. P.; Malrieu, J. P. Ab initio direct calculation of the singlet-triplet separation in cupric acetate hydrate dimer. *J. Am. Chem. Soc.* **1981,** *103*, 4007-4016.

146. van Oosten, A. B.; Broer, R.; Nieuwpoort, W. C. Heisenberg exchange enhancement by orbital relaxation in cuprate compounds. *Chem. Phys. Lett.* **1996,** *257*, 207-212.

147. Cabrero, J.; Ben Amor, N.; de Graaf, C.; Illas, F.; Caballol, R. Ab Initio Study of the Exchange Coupling in Oxalato-Bridged Cu(II) Dinuclear Complexes. *J. Phys. Chem. A* **2000,** *104*, 9983-9989.

148. Stein, C. J.; Reiher, M. Automated Selection of Active Orbital Spaces. *J. Chem. Theory Comput.* **2016,** *12*, 1760-1771.

149. Kittel, C. Model of Exchange-Inversion Magnetization. *Phys. Rev.* **1960,** *120*, 335-342.

150. Huang, N. L.; Orbach, R. Biquadratic Superexchange. *Phys. Rev. Lett.* **1964,** *12*, 275-276.

151. Moreira, I. d. P. R.; Suaud, N.; Guihéry, N.; Malrieu, J. P.; Caballol, R.; Bofill, J. M.; Illas, F. Derivation of spin Hamiltonians from the exact Hamiltonian: Application to systems with two unpaired electrons per magnetic site. *Phys. Rev. B* **2002,** *66*, 134430.

152. Bencini, A.; Totti, F. On the importance of the biquadratic terms in exchange coupled systems: A post-HF investigation. *Inorg. Chim. Acta* **2008,** *361*, 4153-4156.

153. Battaglia, L. P.; Corradi, A. B.; Menabue, L. Structure–magnetism correlation in dimeric copper(II) carboxylates: crystal and molecular structure of tetra-μ-(propanoato-O,O′)-bis[aquacopper(II)]. *J. Chem. Soc., Dalton Trans.* **1986**, 1653-1657.

154. Gerloch, M.; Harding, J. H. Superexchange in copper acetates. *Proc. R. Soc. London, A* **1978,** *360*, 211-227.

155. Boguslawski, K.; Tecmer, P. Orbital entanglement in quantum chemistry. *Int. J. Quantum Chem.* **2015,** *115*, 1289-1295.

156. de Graaf, C.; Sousa, C.; de P. R. Moreira, I.; Illas, F. Multiconfigurational Perturbation Theory: An Efficient Tool to Predict Magnetic Coupling Parameters in Biradicals, Molecular Complexes, and Ionic Insulators. *J. Phys. Chem. A* **2001,** *105*, 11371-11378.

157. Muñoz, D.; De Graaf, C.; Illas, F. Putting error bars on the *ab Initio* theoretical estimates of the magnetic coupling constants: The parent compounds of superconducting cuprates as a case study. *J. Comput. Chem.* **2004,** *25*, 1234-1241.

158. Yanai, T.; Kurashige, Y.; Neuscamman, E.; Chan, G. K.-L. Multireference quantum chemistry through a joint density matrix renormalization group and canonical transformation theory. *J. Chem. Phys.* **2010,** *132*, 024105.

159. Yanai, T.; Kurashige, Y.; Mizukami, W.; Chalupský, J.; Lan, T. N.; Saitow, M. Density matrix renormalization group for ab initio Calculations and associated dynamic correlation methods: A review of theory and applications. *Int. J. Quantum Chem.* **2015,** *115*, 283-299.

160. Schapiro, I.; Sivalingam, K.; Neese, F. Assessment of *n*-Electron Valence State Perturbation Theory for Vertical Excitation Energies. *J. Chem. Theory Comput.* **2013,** *9*, 3567-3580.

161. Fracchia, F.; Cimiraglia, R.; Angeli, C. Assessment of Multireference Perturbation Methods for Chemical Reaction Barrier Heights. *J. Phys. Chem. A* **2015,** *119*, 5490-5495.

162. Freitag, L.; Knecht, S.; Angeli, C.; Reiher, M. Multireference Perturbation Theory with Cholesky Decomposition for the Density Matrix Renormalization Group. *J. Chem. Theory Comput.* **2017,** *13*, 451-459.

163. Kutzelnigg, W.; Mukherjee, D. Cumulant expansion of the reduced density matrices. *J. Chem. Phys.* **1999,** *110*, 2800-2809.

164. Zgid, D.; Ghosh, D.; Neuscamman, E.; Chan, G. K.-L. A study of cumulant approximations to *n*-electron valence multireference perturbation theory. *J. Chem. Phys.* **2009,** *130*, 194107.

165. Andersson, K.; Malmqvist, P. A.; Roos, B. O.; Sadlej, A. J.; Wolinski, K. Second-order perturbation theory with a CASSCF reference function. *J. Phys. Chem.* **1990,** *94*, 5483-5488.

166. Queralt, N.; Taratiel, D.; de Graaf, C.; Caballol, R.; Cimiraglia, R.; Angeli, C. On the applicability of multireference second-order perturbation theory to study weak magnetic coupling in molecular complexes. *J. Comput. Chem.* **2008,** *29*, 994-1003.

167. de Graaf, C.; Hozoi, L.; Broer, R. Magnetic interactions in calcium and sodium ladder vanadates. *J. Chem. Phys.* **2004,** *120*, 961-967.

168. Kurashige, Y.; Yanai, T. Second-order perturbation theory with a density matrix renormalization group self-consistent field reference function: Theory and application to the study of chromium dimer. *J. Chem. Phys.* **2011,** *135*, 094104.

169. Saitow, M.; Kurashige, Y.; Yanai, T. Multireference configuration interaction theory using cumulant reconstruction with internal contraction of density matrix renormalization group wave function. *J. Chem. Phys.* **2013,** *139*, 044118.

170. Sharma, S.; Chan, G. K.-L. Communication: A flexible multi-reference perturbation theory by minimizing the Hylleraas functional with matrix product states. *J. Chem. Phys.* **2014,** *141*, 111101.

171. Veis, L.; Antalík, A.; Brabec, J.; Neese, F.; Legeza, Ö.; Pittner, J. Coupled Cluster Method with Single and Double Excitations Tailored by Matrix Product State Wave Functions. *J. Phys. Chem. Lett.* **2016,** *7*, 4072-4078.

For Table of Contents Only

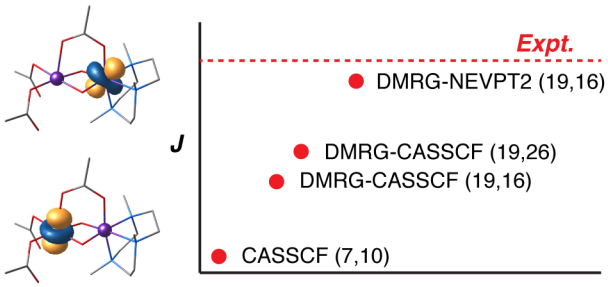

The exchange coupling in a mixed-valence manganese(III,IV) dimer is studied using DMRG-CASSCF and DMRG-NEVPT2 approaches.